8

Comets and asteroids

INTRODUCTION

Comets originate from the Oort Cloud, which is an area of icy debris beyond the orbit of Pluto. Comets are captured and brought into the inner solar system mainly by the gravitational attraction of Jupiter. Here, these comets tend to disintegrate over successive orbits, producing a large number of smaller active comets and inactive asteroids. Many asteroids orbit close to the Earth and in a significant number of cases intersect the Earth's orbit. The population of near Earth objects (NEOs) is replenished discontinuously over time. If an asteroid explodes in the atmosphere it is called a bolide. Our present era is under the influence of a large comet that entered the inner solar system within the last 20,000 years. This chapter looks at the formation of near Earth objects, the probability of their impact with the Earth, the effect of resulting tsunami, and evidence for their occurrence in recent times.

NEAR EARTH OBJECTS (NEOS)

What are they?

(Asher *et al.*, 1994; Steel, 1995; Verschuur, 1996; Lewis, 1999)

There are two main classes of celestial objects: asteroids and comets that can cross the Earth's orbit and eventually impact with the Earth. Asteroids mainly orbit the Sun between Mars and Jupiter. Because of Jupiter's gravitational influence, debris in this region was prevented from agglomerating into a planet, although there is sufficient evidence to suggest that many objects in the asteroid belt have collided with each other. Over 20,000 objects ranging in diameter from several meters to over 1,000 km have been discovered in the asteroid belt. The density of these objects is similar to that of igneous rock. Jupiter still exerts an attraction on asteroids and has the potential to

destabilize them into Earth-crossing orbits. Four groups of asteroids have near Earth orbits. The Apollos, the first group, cross the Earth's orbit but spend most of their time just beyond it. Their orbital period around the Sun is greater than one year. The Amors, the second group, orbit farther out, crossing the orbit of Mars as well as that of the Earth. These objects have unstable orbits, and they are affected the most by the gravity of Jupiter. The Atens, the third class of asteroids, spend most of their time inside Earth's orbit. Their orbital period about the Sun is less than one year. These latter objects were only discovered in the 1970s. A fourth group of asteroids is suspected. These asteroids lie close to the Earth and are thought to originate from debris remaining from asteroid impacts with the Moon.

Comets enter the inner solar system from the Kuiper belt lying outside the orbit of Neptune or from the Oort belt lying beyond the outer boundary of the solar system. The gravitational attraction of Jupiter and Saturn can force a comet as large as 200 km in diameter to traverse the inner part of the solar system once every 200,000 years. There are three types of comets: short, intermediate, and long period. Short-period comets orbit the Sun with periods of less than 20 years. They are called Jupiter family comets because they come under the gravitational influence of Jupiter and have unstable orbits. The best example is Comet P/Encke. Intermediate-period or Halley-type comets have orbital periods between 20 and 200 years. Long-period comets have orbital periods greater than 200 years and tend to appear in the inner solar system only once.

The best-known comet to impact with the Earth occurred at Chicxulub on the Yucatan Peninsula of Mexico at the Cretaceous–Tertiary boundary (Figure 8.1). This event threw up large volumes of sediment into the stratosphere, attenuated solar radiation significantly for months, if not years, and led to the extinction of the dinosaurs. Comets consist mainly of ice and stony or iron material ranging in size from sand grains to boulders hundreds of meters in diameter. As comets approach the Sun, they slowly disintegrate as ice is vaporized and discharged with other gases in a tail that can extend millions of kilometers into space. There is growing evidence that comets are responsible for much of the debris orbiting the inner solar system. Some main-belt asteroids may be the remnants of comets, and most of the Earth-crossing asteroids have short-lived orbits about the Sun, suggesting that they too originated from the breakup of comets. The Earth is known to cross through at least 12 comet debris trails that form prominent meteorite showers.

The most important comet stream is the Taurid complex. It is theorized that a large comet, about 100 km in diameter, initially entered the inner solar system 20,000 years ago and began to break up about 14,000 years ago. Further disintegration events occurred around 7500 BC and 2600 BC. The latter breakup happened during the Bronze Age and was associated with asteroid strikes within the next few centuries that impacted dramatically upon civilizations. Debris from the disintegration forms the Taurid complex, which consists of a dozen asteroid objects 0.5 km–2.0 km in diameter. There may be another hundred objects in this size range yet to be discovered in the complex. As well, probably only 1%–2% of Taurid objects smaller than 0.5 km in size have been detected to date. The breakup of the original comet also generated four prominent meteor showers appearing annually with a major peak in

Figure 8.1. An artist's impression of the Chicxulub impact tsunami as it crossed the coastal plain of the United States. The impact event was responsible for the extinction of the dinosaurs, 65 million years ago. The figure appeared originally in Alvarez (1997). See color section. © Ron Miller 1997 and reprinted by permission.

October–December and a minor peak in April–June. One prominent reactivated comet, P/Encke, is also part of the Taurid complex. Comet P/Encke first appeared in 1786 following the last large display of meteorites associated with the Taurids. Comet P/Encke is about 5 km in diameter, has a mass of 1,013 tonnes, and orbits the Sun every 3.5 years in an Earth-crossing orbit. The Taurid complex also contains other large objects that presently have orbits that intersect the Earth in the last few days of June each year. The Tunguska airburst of June 30, 1908 was a Taurid object, as was a 1 km sized object that struck the far side of the Moon on June 19, 1178. This latter event produced the 20 km diameter Giordano Bruno crater as well as spreading dust across the face of the New Moon, splitting the upper horn with flame, and causing the Moon to "throb like a wounded snake". The Monk Gervasse, in Kent, who saw the sequence repeatedly several times, witnessed the event. This latter description also appears in Maori legends in New Zealand. The event itself may have sent debris crashing into the Earth several days latter.

The perceived view that relatively small NEOs hundreds of meters in size are innocuous is misleading. For example, a 100 m to 500 m diameter object moving at a velocity of 30 km s^{-1} will release energy equivalent to 100–30,000 megatons of TNT. The large asteroid 1989FC, which was 500 m in diameter and missed the Earth by 650,000 km, would have destroyed civilization if it had hit our planet. It would have

created a crater about 10 km in diameter, released energy equivalent to the world's total nuclear arsenal, triggered an earthquake with a hypothesized magnitude, M_s, of 9–10, spread a hot plume burning tens of thousands of square kilometers of forest, ejected billions of tonnes of rocks and dust into the atmosphere with consequent lowering of temperatures and partial blocking of photosynthesis for several years, induced acid rain due to atmospheric reaction of nitrogen and oxygen, and depleted ozone in the stratosphere.

How frequent have comet and asteroid impacts been?

(Rasmussen, 1991; Hasegawa, 1992; Asher and Clube, 1993; Asher *et al.*, 1994; Steel, 1995; Verschuur, 1996; Lewis, 1999)

It is estimated that, since hominids evolved, between 200 and 500 extraterrestrial bodies several hundred meters in size have impacted with the Earth. About 70% of NEOs are asteroids, of which 50% are derived originally from comets. The best approximation of the probability of impact with the Earth of various sizes of objects is presented in Figure 8.2. There are large uncertainties, spanning an order of magnitude, on the return period of these objects because the total population of NEOs is presently unknown. Observations of the more frequent, smaller iron meteorites and bolides are also uncertain because historical records beyond a few centuries are very limited globally. The range in kinetic energy presented in Figure 8.2 reflects the range in speed of objects striking the Earth—typically between $10\,\mathrm{km\,s^{-1}}$ and $45\,\mathrm{km\,s^{-1}}$. Astronomical observations indicate that one to three near Earth objects with a diameter of 1 km could impact the Earth every 100,000–200,000 years. This size object is undoubtedly more common than present observations indicate and may occur every 50,000 years. An object 50 m in diameter crashes into the Earth every century while a Tunguska-sized object of 60 m diameter occurs every 200–300 years.

These probabilities may be conservative because they are based upon recorded events rather than the probable population of NEOs. Simulations have been made of the number of types of impacts that could randomly be expected over a period of 10,000 years. Over this timespan, there could be 110 impact events, 285 Tunguska style airbursts over land, 680 over the ocean, and 12 ocean impacts that could produce ocean-wide tsunami. Only four events would be big enough to leave a crater on land, and all of these would have a high probability of being eroded or buried.

Of the Tunguska-sized events, one or two impacts would have been equivalent to 500–1,000 megatons of TNT. Their impacts must have affected global climate and the course of human history. All of the Tunguska-sized objects that strike the ocean could have generated significant tsunami. Gerrit Verschuur makes the interesting comment that, historically, few population centers existed around the shores of the Atlantic or Pacific Oceans. The cradles of civilization emerged in relatively sheltered river valleys around smaller seas—the Mediterranean, Red Sea, and Persian Gulf, or in mountain regions such as the Andes and the south Indian highlands. Our ancestors may have been wiser than we are and avoided coastal areas because of the potentially devastating effects of asteroid-generated tsunami that were occurring at regular intervals in circum-oceanic regions.

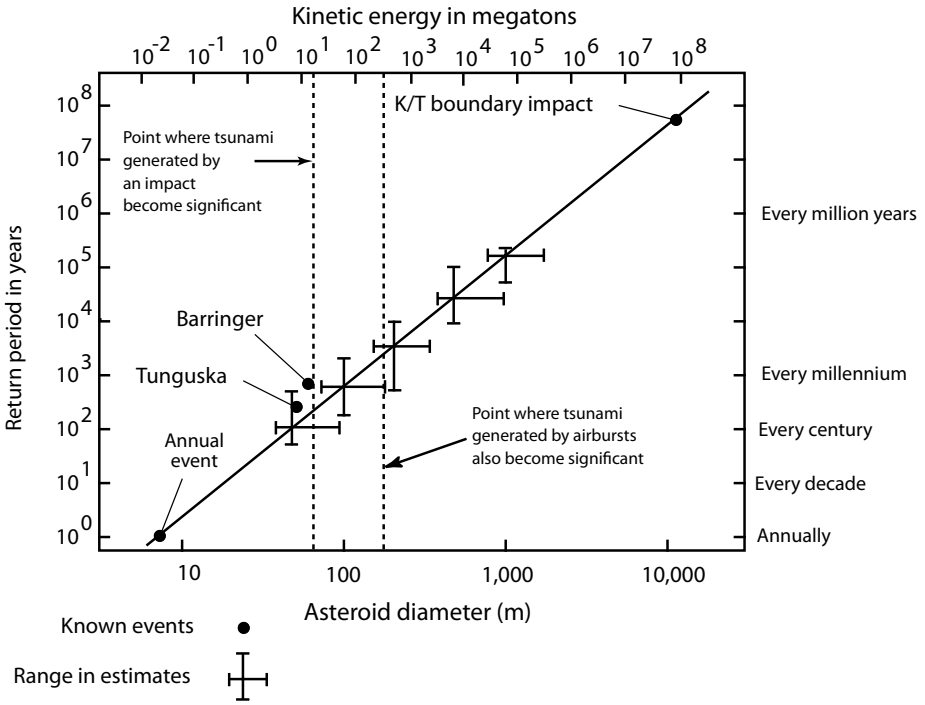

Figure 8.2. Probability of comets or asteroids of given diameter striking the Earth. Based on Verschuur (1996) and formulas presented in this chapter. Estimates derived from Michael Paine's web page at *http://users.tpg.com.au/users/tps-seti/spacegd7.html#impacts*.

These probabilities also assume a random but constant flux of objects intersecting the Earth. However, the appearance of comets and asteroids in the inner solar system, and their impact with the Earth, is clustered in time in a phenomenon astronomers call coherent catastrophism. This is logical when it is realized that cometary disintegration leads to the production of objects 10 m–100 m in size, with some kilometer-sized objects orbiting about the Sun within the confines of a narrow stream or trail. These objects tend to be clustered within this stream. Resonant interaction by Jupiter and the inner planets upon a stream such as the Taurid complex periodically allows objects within the stream to intersect the Earth's orbit, leading to multiple bombardments of Tunguska-sized objects (or larger) over periods of one to four centuries. In terms of global catastrophes, it is not the random impact of celestial objects greater than 1 km in diameter occurring on average every hundred thousand years that is important, but rather the occurrence of clusters of Tunguska-sized objects during epochs of high activity. The latter can affect civilizations deleteriously through direct impact, the generation of tsunami, or modifications to the atmosphere leading to sudden periods of global cooling.

Some measure of coherence in meteorites and comets can be obtained from Chinese, Japanese, and European records of meteor, comet, and fireball sightings

gathered over the last 2,000 years. The accumulated record, up to the beginning of the 19th century when scientific observations began in earnest, is plotted in Figure 8.3. The Asian records are the most complete, with European sightings accounting for less than 10% of the record over the last thousand years. The comet observations from Asia are also plotted in Figure 8.3. A quasi-cyclic pattern is evident in the records that can be linked to the dominance of the Taurid complex in the inner solar system. Peak occurrences of cosmic input to the atmosphere occurred between 401 and 500; 801 and 900; 1041 and 1100; 1401 and 1480; 1641 and 1680; and 1761 and 1800. These intervals have been shaded. The first period corresponds with the last extended epoch of nodal intersection with the Taurid complex, while the prominent fluxes in the 11th and 15th centuries correspond to nodal intersections with parent objects in the complex. The 15th century represents the last phase of coherent catastrophism associated with the Taurid complex. In addition, there is a preference for sightings to occur in July–August and October–November. Some astronomers believe that many of these peaks were responsible for the climate changes and direct impacts that have affected the course of human history.

HOW DO EXTRATERRESTRIAL OBJECTS GENERATE TSUNAMI?

Mechanisms for generating tsunami

(Chyba, Thomas, and Zahnle, 1993; Nemtchinov, Loseva, and Teterev, 1996; Verschuur, 1996)

There are four types of extraterrestrial objects based upon density: comets ($\sim$1.0 g cm^{-3}), carbonaceous bodies (2.2 g cm^{-3}), stony asteroids (3.5 g cm^{-3}), and iron asteroids (7.9 g cm^{-3}). Comets are generally considered dirty snowballs; however, larger comets, in breaking up in successive orbits within the inner solar system, may produce many of the asteroids of various densities that strike the Earth. These four classes of objects also have different yield strengths that can vary over several orders of magnitude. The yield strength determines how easily the objects will fragment when they hit the atmosphere. Finally, these objects travel through space at different speeds. Comets travel at 25 km s^{-1}–50 km s^{-1}, while the near Earth objects move at slower speeds of 15 km s^{-1}. If objects fragment and explode in the atmosphere as bolides before striking the Earth's surface, they can still generate tsunami. In this case the size of the wave depends very much upon the height of the explosion in the atmosphere.

Any object greater than 1 km in diameter tends to intersect the Earth's atmosphere without fragmenting or exploding. In effect, these large objects travel fast enough that they do not have time to see the atmosphere before striking the surface. Comets less than 580 m in diameter, and stony and iron asteroids less than 320 m and 100 m in diameter, respectively, begin to distort or fragment traveling through the atmosphere. Any object entering the atmosphere at a shallow angle is more likely to reach the ocean without breaking up; however, this doesn't necessarily lead to bigger tsunami. Distortion without fragmentation leads to a pancake-shaped

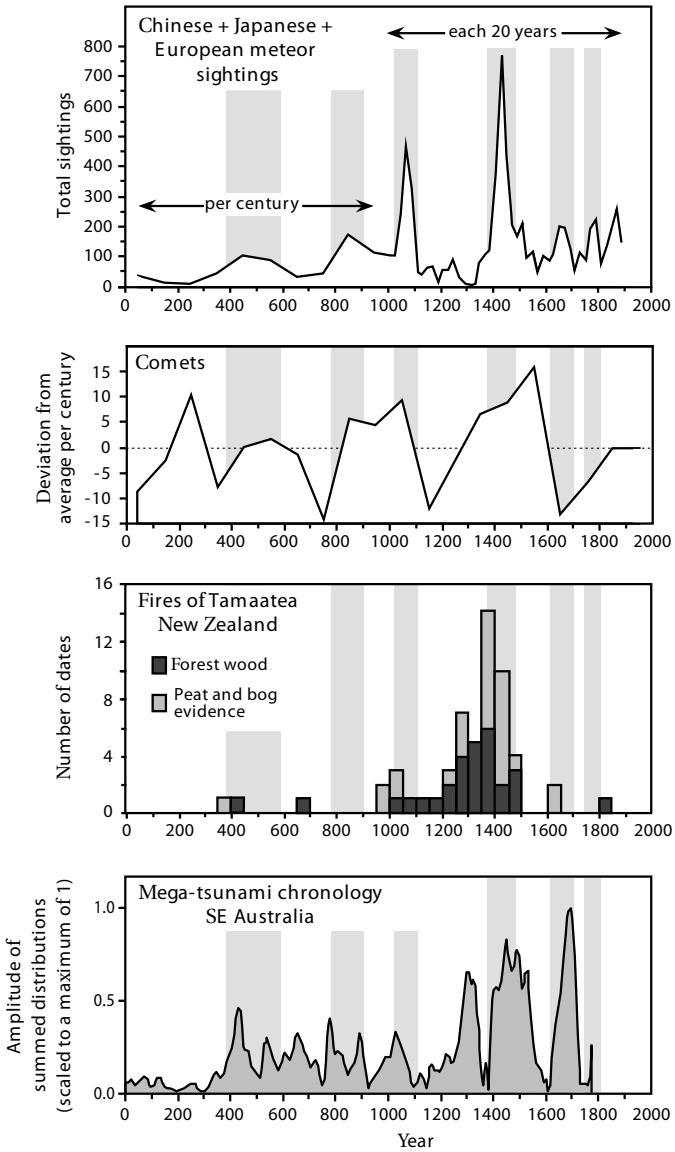

Figure 8.3. Incidence of comets and meteorites, and related phenomena, between AD 0 and AD 1800. The meteorite records for China and Japan are based on Hasegawa (1992), while meteorite records for Europe come from Rasmussen (1991). Peak occurrences are shaded. The Asian comet record is based on Hasegawa (1992). The calibrated radiocarbon dates under the *Mystic Fires of Tamaatea* are from Mooley *et al*. (1963) for forest wood and from McGlone and Wilmshurst (1999) for peats and bogs. The chronology of mega-tsunami is based on 29 radiocarbon dates of marine shell with five additional AMS dates from the Tura region of New South Wales. See text for an explanation on how this time series was constructed. The dips over the last millennium are an artifact of age reversals in radiocarbon chronology.

body of greater diameter impacting into the ocean. Even if an asteroid fragments, the fragments can hit the ocean as a hollow shell, creating a cavity that can be ten times greater than the radius of the original asteroid or comet. Theoretically, an iron meteorite with a diameter of less than 30 m could generate a tsunami by this mechanism. The initial waves formed in this case are technically not tsunami, as they are formed by the air blast. The real tsunami comes about 5 seconds later when the cavity in the water collapses. These fragmentation and distortion aspects have not yet been modeled in the generation of tsunami, but may be very important.

Under fragmentation, a tsunami wave can be created by a minimum expenditure of 2–4 megatons of energy. The Tunguska airburst occurred at 7:40 AM on June 30, 1908, flattening radially 2,150 km^2 of forest near the Podkamennaya Tunguska River, in central Siberia (60°55′N, 101°57′E). The explosion was equivalent to 10–20 megatons of TNT released into the atmosphere at an elevation of 8 km–9 km. This was one thousand times more than the Hiroshima atomic bomb. The air blast that reached the ground had only 1% of the bolide's kinetic energy—equivalent to about 0.1–0.2 megatons of TNT. The object must have been a small comet with a diameter of 60 m traveling at a velocity of 15 km s^{-1}. If the object had been an iron asteroid, then it needed to be traveling at a higher speed of 30 km s^{-1}–40 km s^{-1} in order to explode at this height. Such an event is too rare, because this high velocity excludes about 90% of all known Earth-crossing asteroids. If the object had been a stony asteroid, then some debris would have reached the ground. None did.

Asteroid-generated tsunami can be modeled using the same incompressible, shallow-water long-wave equations described in Chapter 2. In fact, meteoritic tsunami are similar to those generated by rockfalls such as the Lituya Bay tsunami of July 9, 1958 discussed in Chapter 6. For example, a small meteoroid of only 500 m diameter falling in the ocean at 20 km s^{-1}, at a low angle of entry, could carve a path at least 12 miles long across the ocean. The horizontal and vertical accelerations of the resulting seismic waves would be much greater than any known earthquake. An important similarity between low-angled asteroid impacts and the Lituya rockfall-induced tsunami is the role played by splash. Low-trajectory asteroids can eject into the atmosphere enormous volumes of water that travel at high velocities, travel hundreds of kilometers, and fall back to the surface of the Earth over equivalent distances (Figure 8.4). This splash can emulate the erosional effects of tsunami and may be far more important as a geomorphic process of asteroid impacts than any tsunami generated by cratering in the ocean. The significance of such events will be described later in this chapter.

Size of tsunami

(Shoemaker, 1983; Huggett, 1989; Nemtchinov, Loseva, and Teterov, 1996; Verschuur, 1996; Goodman, 1997; Hills and Mader, 1997; Toon *et al.*, 1997; Crawford and Mader, 1998; Paine, 1999; Ward and Asphaug, 2000)

As a rough approximation, the height of a tsunami generated by an asteroid impact with the ocean can be determined by relating its kinetic energy to that of known tsunami generated by earthquakes and volcanoes. For example, the Chilean earth-

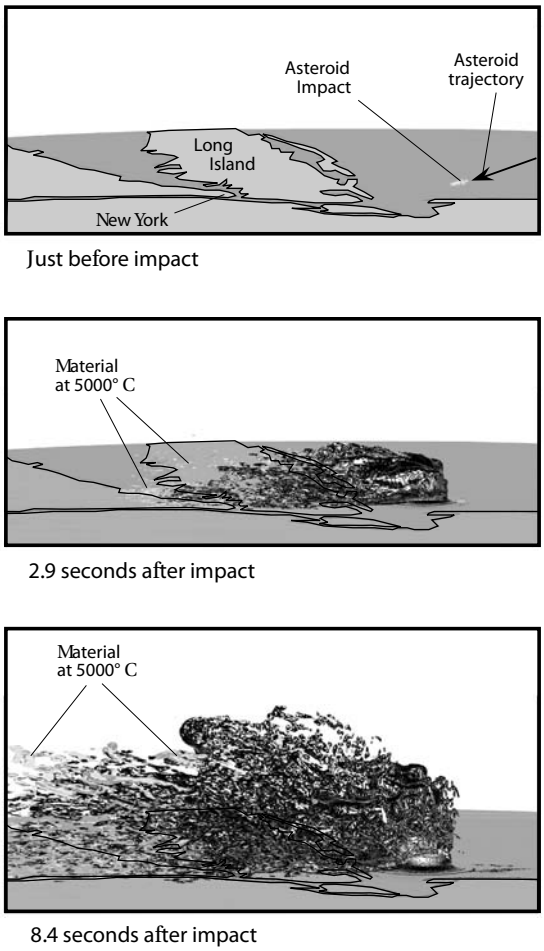

Figure 8.4. Computer simulation of the splash from an asteroid striking the ocean off the coast of Long Island. The asteroid is 1.4 km in diameter and is traveling northward at a speed of 20 km s^{-1}. Note the vapor heated over 5,000°C. Dark material is water vapor; white material is water. The simulations were performed at Sandia National Laboratories using an Intel Teraflops supercomputer. They took 18 hours to complete. Images are used courtesy Dr. David Crawford. More images and movies are located at *http://www.sandia.gov/media/comethit.htm*

quake of 1960 generated a tsunami with kinetic energy equivalent to 2–5 megatons of TNT, while the Alaskan earthquake of 1964 generated a tsunami equivalent to 0.14 megatons of TNT. The eruption of Krakatau in 1883 was equivalent to 200 megatons of TNT. While not all of this latter energy went into the tsunami, run-up of over 40 m occurred within a 100 km radius. The air blast of the Tunguska bolide at the ocean's surface produced only 0.1–0.2 megatons of energy. This would only have generated a localized tsunami of around 0.2 m in height had it occurred over the ocean. However,

had the comet reached the ocean's surface, it would have created a tsunami with an initial wave height of over 900 m. Thus, most asteroids must be large or dense enough to crash into the ocean without fragmenting in order to produce a significant tsunami.

Of the asteroids or comets that reach the Earth's surface, about 70% will strike the ocean. At velocities of over 20 km s^{-1}, these objects burst upon contact with the ocean, sending out splash that can reach the top of the atmosphere. Collapse of water back into the cavity left by the impact creates a tsunami wave train. The height of the tsunami wave depends upon the displacement of water from the pseudo-crater blasted into the ocean. The volume of water absorbs most of an asteroid's energy so that no imprint or crater is left behind on the seabed. The displaced water piles up around the crater and forms a ring whose width equals the radius of the crater. The tsunami's wave height can be approximated initially by the following formula:

$$H_m = rdR_t^{-1} \tag{8.1}$$

where H_m = height of the tsunami wave above mean sea level (m)
r = the radius of the pseudo-crater in the ocean (m)
R_t = the distance from the center of impact (m)
d = water depth (m)

As this ring moves out from the center of impact, it causes water to oscillate up and down, forming about four ringlets that propagate outward as a tsunami wave train. This process is similar to the ripples that form when a pebble is thrown into a pond. As the wave moves away from the impact site, its height then becomes dependent upon the distance from the center of impact. Shoemaker proposed a simple formula, based upon analogies to nuclear explosions, to estimate the size of the crater generated by any asteroid as follows:

$$D = SpW^{0.3} \tag{8.2}$$

where D = diameter of an impact crater (m)

$$Sp = 90\rho_e^{0.3}$$
$$= \text{density correction} \tag{8.3}$$

where ρ_e = density of material ejected from an impact crater (g cm^{-3})

$$W = 0.12 \times 10^{-12} m v_a^2$$
$$= \text{kinetic energy of impact (kilotons of TNT)} \tag{8.4}$$

where v_a = impact velocity of asteroid (m s^{-1})

$$m = 1.33\pi\rho_a r_a^3$$
$$= \text{mass of asteroid (kg)} \tag{8.5}$$

where r_a = radius of asteroid (m)
ρ_a = density of asteroid (g cm^{-3})

Using Equation (8.4), the kinetic energy of an iron meteorite 40 m in diameter with a density of 7.8 g cm^{-3}, traveling at a velocity of 20 km s^{-1} such as that which created the 1.2 km wide Barringer crater in Arizona—is equivalent to 12.5 megatons of TNT. Equations (8.2) and (8.3) indicate that this object would have produced a pseudo-crater 1.5 km in diameter if it had hit the ocean.

When Equation (8.2) is substituted into Equation (8.1), the size of the tsunami is over-estimated for small asteroids. Equation (8.1) also does not account adequately for tsunami generated by stony asteroids or asteroids in shallow seas. Stony asteroids smaller than 100 m in diameter tend to fragment in the ocean. Larger ones tend to dissipate some of their energy in the atmosphere. For example, a 200 m diameter stony asteroid traveling at 25 km s^{-1} would impact with a force equivalent to 940 megatons of TNT. If this asteroid exploded as an airburst, then only 20% of its energy would reach the surface of the ocean. This latter component is more than 30 times greater than the energy of the Chilean tsunami of 1960 and approximately equal to the largest Krakatau eruption of 1883. The diameter of the smallest object that can reach the Earth's surface virtually intact is 40 m for an iron meteorite, 130 m for a stony asteroid, and 380 m for a short-period comet. The recurrence interval for a stony asteroid, 130 m in diameter, is about every thousand years. The tsunami created by large asteroids impacting in the ocean are also depth limited. As a rule of thumb, depth becomes a limiting factor when it is less than 12 times the diameter of the asteroid. For example, asteroids greater than 167 m in diameter will be depth limited if the asteroid falls into water less than 2,000 m deep. In this case, the resulting tsunami is 60% smaller than if the asteroid had fallen into deeper water. Stony asteroids also produce waves that are 60% smaller than those produced by denser asteroids. The following equations more realistically model these three conditions:

$$\text{Iron asteroid:} \quad H_m = 1.87 W^{0.54} R_t^{-1} \tag{8.6}$$

$$\text{Stony asteroid:} \quad H_m = 3{,}900[(0.005 r_a)^3 (0.05 v_a)^2 (0.33 \rho_a)]^{0.54} R_r^{-1} \tag{8.7}$$

$$\text{Shallow water:} \quad H_m = 0.0229 W^{0.25}\, d R_t^{-1} \tag{8.8}$$

These relationships are tabulated for asteroids of between 0.1 km and 1.0 km in diameter in Table 8.1. The heights of tsunami produced by an iron asteroid are also plotted in Figure 8.5. This size range covers those objects that could realistically strike the Earth's ocean in the near future. Tsunami wave height quickly attenuates away from the site of impact. It also increases sizably as the diameter of the asteroid increases. For example, a 100 m diameter iron asteroid would produce tsunami of 27.1 m, 2.7 m, and 0.7 m in height, within 50 km, 500 km, and 2,000 km, respectively, of the center of impact. This size asteroid is the minimum limit presently proposed for the detection of NEAs and one equivalent in energy to the Krakatau eruption of 1883. The wave heights are equivalent to tsunami generated by the Krakatau eruption over similar distances. The 0.7 m height is much higher than the 0.2 m to 0.4 m open ocean height postulated for the Chilean tsunami of 1960, 2,000 km away from its source. As mentioned in Chapter 5, this latter tsunami's run-up measured 3 m high

Table 8.1. Tsunami heights generated at distances of 50 km, 500 km, and 2,000 km from the impact site of iron or stony asteroids with the ocean.

Iron asteroid characteristics				*Tsunami height* (m)					
				Iron asteroid			*Stony asteroid*		
Asteroid diameter (m)	*Kinetic energy* (Mt TNT)	*Kinetic energy* ($J \times 10^{18}$)	*Crater diameter* (km)	*50 km distance*	*500 km distance*	*2,000 km distance*	*50 km distance*	*500 km distance*	*2,000 km distance*
100	198	1	3.4	27.1	2.7	0.7			
150	667	3	4.9	52.2	5.2	1.3	15.5	1.6	0.4
200	1,581	7	6.3	83.3	8.3	2.1	24.8	2.5	0.6
250	3,089	13	7.7	119.5	12.0	3.0	35.6	3.6	0.9
300	5,337	22	9.1	160.6	16.1	4.0	47.8	4.8	1.2
350	8,475	35	10.5	206.1	20.6	5.2	61.3	6.1	1.5
400	12,651	53	11.8	255.9	25.6	6.4	76.1	7.6	1.9
450	18,013	75	13.1	309.7	31.0	7.7	92.1	9.2	2.3
500	24,710	103	14.4	367.3	36.7	9.2	109.3	10.9	2.7
550	32,889	138	15.7	428.7	42.9	10.7	127.5	12.8	3.2
600	42,699	179	17.0	493.6	49.4	12.3	146.9	14.7	3.7
650	54,288	227	18.3	561.9	56.2	14.0	167.2	16.7	4.2
700	67,804	284	19.5	633.6	63.4	15.8	188.5	18.9	4.7
750	83,396	349	20.8	708.5	70.8	17.7	210.8	21.1	5.3
800	101,212	424	22.0	786.6	78.7	19.7	234.0	23.4	5.9
850	121,400	508	23.2	867.7	86.8	21.7	258.2	25.8	6.5
900	144,108	603	24.5	951.9	95.2	23.8	283.2	28.3	7.1
950	169,485	709	25.7	1,039.1	103.9	26.0	309.2	30.9	7.7
1,000	197,679	827	26.9	1,129.1	112.9	28.2	336.0	33.6	8.4

Note: Velocity of impactor = 20 km s^{-1}; density of iron asteroid = 7.9 g cm^{-3}; density of stony asteroid = 3 g cm^{-3}; ocean depth at impact = 5,000 m.
Source: Based on Shoemaker (1983), and Hills and Mader (1997).

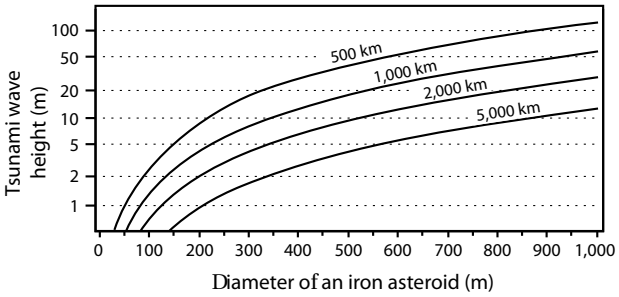

Figure 8.5. The size of tsunami generated by iron asteroids of various diameters striking the ocean. The heights are at distances of 500 km, 1,000 km, 2,000 km, and 5,000 km from the center of impact. The asteroids have a density of 7.8 g cm^{-3} and impact with a velocity of 20 km s^{-1}.

on the Hawaiian Islands and 1 m–2 m in Japan, and killed 61 and 190 people, respectively, in each area.

If the height of a tsunami at shore were approximately ten times its open ocean height, then according to Equation (2.14), the tsunami wave produced by a 100 m diameter iron asteroid would penetrate inland 890 m on any flat coastal plain within 2,000 km of the impact. An iron asteroid 500 m in size can generate a tsunami wave that is approximately 35 m high leaving the impact site. Two thousand kilometers away, this tsunami would still be approximately 10 m high. If this size asteroid landed in the middle of the Pacific Ocean, its tsunami would be just less than 5 m in height approaching any of the surrounding coastlines. Theoretically, this wave could sweep inland over 12 km across any flat coastal plain in the Pacific Ocean region. Stony asteroids are less effective at generating tsunami than iron asteroids, but the impact of their run-up is just as impressive. A 500-m stony asteroid would generate a tsunami that is 2.7 m high, 2,000 km from the impact site. This is bigger than any historical tsunami in the Pacific. Such a wave could sweep inland 5.3 km over any flat coast surrounding the Pacific Ocean.

Asteroids larger than 1 km in diameter will produce catastrophic tsunami in any ocean. Simulations have been performed on the effects of an asteroid 5 km in diameter falling into the mid-Atlantic or west Pacific Ocean. Such objects have a return period of once every 10 million years. At 1,000 km from the impact site, the resulting tsunami would be over 45 m high. At 2,000 km distance, the wave would begin to shoal onto continental shelves with a height of 22 m. Modeling, using incompressible, shallow-water long-wave equations indicates that a significant amount of this wave's energy would be reflected from the front of flat continental shelves. Hence, coasts protected by wide shelves, such as those found along the east coast of the United States and northern Europe, are less affected by cosmogenic tsunami than are steep coasts such as those found along the coasts of Australia or Japan. However, even on the most protected coastline, the wave formed by an asteroid more than 5 km in diameter would be 30 m or more high.

Recent mathematical and computer modeling indicates that there is a wide range in the calculated heights of tsunami emanating from asteroid impacts. Figure 8.6

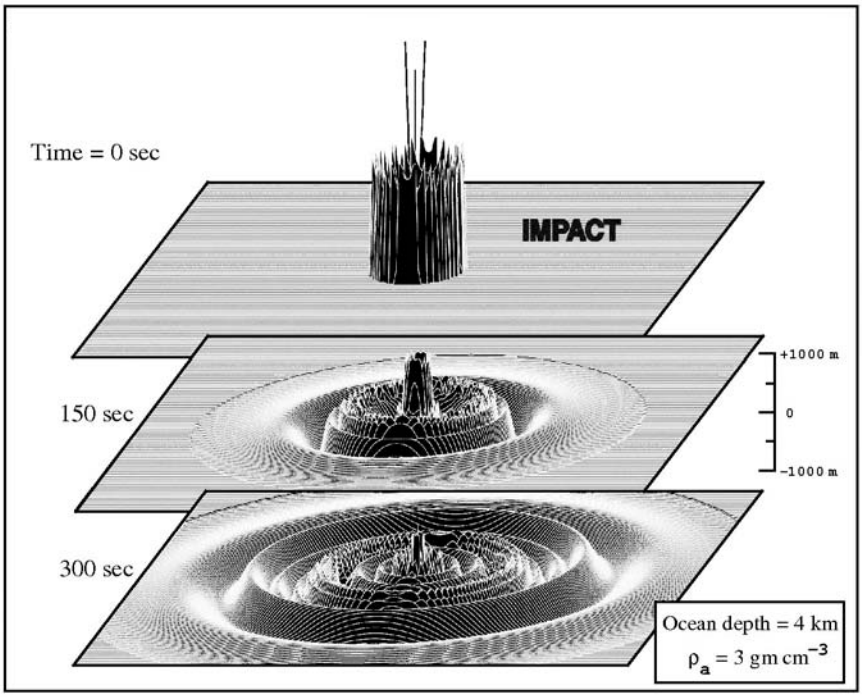

Figure 8.6. Modeled results of the initial development of a tsunami created by the impact of a 200 m diameter stony asteroid with a density of 3 g cm^{-3} traveling at 20 km s^{-1}. Within 300 s, a tsunami propagates outward more than 50 km. The leading wave in the bottom panel is about 325 m high. Based on Ward and Asphaug (2000). Dr. Steven Ward, Institute of Tectonics, University of California at Santa Cruz, kindly provided a digital copy of this simulation.

presents a simulation of the wave height produced by a stony asteroid 200 m in diameter traveling at a speed of 20 km s^{-1}. The leading edge of the resulting tsunami travels 25 km from the center of the impact within 5 minutes and is over 300 m high. At distances of 50 km, 500 km, and 2,000 km the wave is still over 100 m, 11 m, and 6 m high, respectively. These heights are more than four times greater than the calculated heights based upon nuclear explosions (Table 8.1).

At the other extreme, simulations of asteroid impacts into an ocean have been performed on a supercomputer at the Sandia National Laboratories in New Mexico, using algorithms that modeled accurately the impact of the Shoemaker–Levy 9 comet into Jupiter's atmosphere in July 1994. These are the same calculations used in the simulation of splash effects shown in Figure 8.4. Despite an uncertainty factor of 2, the computer modeling yields tsunami heights that are smaller than those derived using Equation (8.6) by a factor of almost 10. These differences are summarized in Table 8.2 for a small range of asteroid sizes. The differences have been calculated 500 km from the center of impact for an iron asteroid striking an ocean 5,000 m deep at a velocity of 20 km s^{-1}. The modeled tsunami wave heights span an order of

Table 8.2. Crater and tsunami characteristics modeled using analogs to nuclear explosions and the Shoemaker–Levy comet impact into Jupiter.

	Asteroid diameter (m)		
	250	*500*	*1,000*
Analog to nuclear explosions			
Crater size (km)	7.7	14.4	26.8
Tsunami height (m)	11.9	36.5	112.1
Sandia computer simulations			
Crater size (km)	5	10	20
Wave velocity ($m\,s^{-1}$)	166	166	900
Wave period (s)	150	180	300
Tsunami height (m)	1.3	5.0	12.0

Note: Latter modeling is the same as that used in Figure 8.4. Wave heights are taken 500 km from the impact site.
Source: Based on Crawford and Mader (1998).

magnitude—a fact indicating that there is not a broad consensus among researchers on the heights of asteroid-generated tsunami.

GEOLOGICAL EVENTS

Hypothesized frequency

(Dypvik and Jansa, 2003; Planetary and Space Science Center, 2007)

Impact craters are profoundly difficult to identify because of active erosion of the Earth's surface and recycling of the Earth's crust through plate tectonics. As of 2007, 174 impact craters have been identified on the surface of the Earth, excluding the polar icecaps. Identification is presently proceeding at the rate of 15 new craters per decade. Only 7 of these are marine, while 19 originally occurred in the ocean, but are now preserved on land. Only marine impacts generate tsunami. While some of the preserved craters may have occurred on the margins of oceans, no deep–ocean basin impact structure has been recognized. Impacts in the ocean produce variable crater forms depending upon the depth of water. Impacts in shallow water produce craters with low or absent rims because currents and back flow into the crater smooth out topography. Such currents can also cut gullies through the crater rim. Infilling of the crater with sediment is also a dominant process, so crater relief is shallow. If an impact occurs on the edge of the continental shelf, then that part of the crater farthest from land may collapse sending shelf material cascading onto abyssal plains to build up sediments hundreds of meters thick. In the deepest ocean, water does not absorb the impact. Here craters are more likely to approximate the shape of those formed on land. The size of the resulting tsunami also varies. Those generated on the continental

shelf or in shallow gulfs and bays may only be 1 m–2 m in height even where craters 10 km in diameter have formed. The resulting features on land cannot be separated easily from those formed by tsunami generated by large earthquakes or submarine slides. Tsunami propagating landward from impacts on the edge of the continental shelf are similar. However, the tsunami propagating seaward from these locations may be much larger and more destructive on distant shores. Impacts in deeper water generate tsunami originating from a point source. Here even small impacts generated by low-density comets 1 km in size may produce tsunami larger than those generated by the greatest earthquakes of the past century. Evidence of such a tsunami should be present basin-wide with features orientated back to a common point source.

Comet and meteor impacts were common in the early history of the Earth, but within the last 225 million years, the Earth has only been struck randomly by debris flung into the inner solar system or by asteroids orbiting between the Earth and Jupiter. One hundred and two craters have been identified over this period, of which 14 have a marine source. By far the largest of these is Chicxulub crater, which is 180 km in diameter and is buried beneath the Yucatan Peninsula in Mexico. Chicxulub is one of the few submarine impacts now preserved under a continent. This event has been linked to the Cretaceous–Tertiary boundary extinction of the dinosaurs 65 million years ago. Chicxulub will be described in more detail subsequently. If the distribution of asteroid impacts was spread evenly over the Earth's surface, and if it can be assumed that the oceans have continually occupied at least 70% of the world's surface area, then a minimum of 205 impacts should have occurred in the oceans over the last 225 million years. This represents approximately one ocean impact event every million years.

It is possible to use Equation (8.2) and the size of known impact craters to calculate the energy released by each impact, and the diameter of the impacting object. In this analysis, it is assumed that all of the objects were iron asteroids with a density of $7.8\,\mathrm{g\,cm^{-3}}$, and that they struck crustal material with a density of $2.65\,\mathrm{g\,cm^{-3}}$. In addition, the diameter of craters larger than 3 km has been adjusted upward by a factor of 1.3 to account for collapse due to gravity. It is possible to use Equations (8.6) and (8.8) to calculate the hypothetical distribution of tsunami wave heights in the ocean produced by this theorized population of impacts over the last 225 million years. This distribution is plotted in Figure 8.7 at a distance of 1,000 km from each impact site. All objects are assumed to have fallen into an ocean that is 5,000 m deep. Shallow-water corrections have been applied where required because they make the theorized tsunami wave heights more realistic. For example, the Chicxulub impact object, which had a postulated diameter as great as 15 km, would have generated a tsunami 4.6 km high without this correction, as opposed to one 104 m high with it. The latter value is closer to estimates derived from analysis of sedimentary deposits laid down by the wave. The average height of theorized, asteroid-generated tsunami waves in the ocean over the past 65 million years is 12.6 m. If the cut-off value for mega-tsunami begins at 5 m, then 40% of impacts generated this type of event. The probability of an asteroid producing a tsunami more than 5 m in height over the next million years is 0.26%. Since civilization began, the probability of such a large event has only been 0.0026%. Mega-tsunami greater than

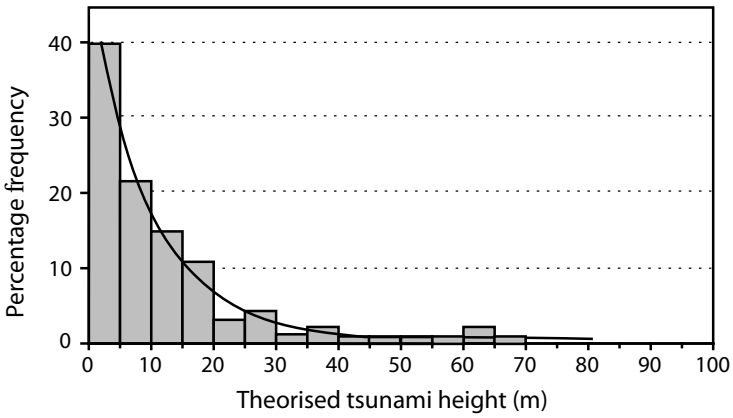

Figure 8.7. Theoretical distribution of tsunami wave heights generated by iron asteroid impacts with the world's oceans over the last 225 million years. Density of the meteorites is 7.8 g cm^{-3}.

20 m in elevation are rare and represent in total 17% of hypothesized events. While the effect of mega-tsunami in any ocean would be catastrophic, geologically they do not appear to have been a dominant force shaping world coastal landscape. This poses a conundrum for the Late Holocene epoch—beginning about 7,000 years ago when sea level reached present levels after the Last Glacial, because evidence of mega-tsunami over this period is more common.

Chicxulub, the Cretaceous–Tertiary (K/T) extinction event

(Bourgeois *et al*., 1988; Smit *et al*., 1996; Verschuur, 1996; Alvarez, 1997)

One of the great mysteries of geology, the extinction of the dinosaurs, was not solved until 1980, when Walter Alvarez and his colleagues proposed that a comet had caused a global winter that not only killed the dinosaurs, but also wiped out 67% of all species at the boundary between the Cretaceous and the Tertiary. That hypothesis was speculative until the crater for the impact was eventually found underlying Chicxulub, on the Yucatan Peninsula in Mexico. Finally, between 1988 and 1992, tsunami deposits were found in the region that linked the Chicxulub crater to what is now called the K/T extinction event.

The comet responsible for the extinction event was about 10 km–15 km in diameter, and produced a crater 180 km in diameter in anhydrite-rich limestones and dolomites. Two fireballs issued from the impact site. The first consisted of a cloud of extremely hot vaporized rock, followed closely by a superheated cloud of CO_2 gas released from the carbonates. The heat was so intense that all vegetation burned out to a radius of several thousand kilometers, loading the atmosphere with soot. Seismic waves with surface wave magnitudes, M_s, of 9–11 caused faulting in shallow waters around the Gulf of Mexico. Huge submarine landslides were triggered on

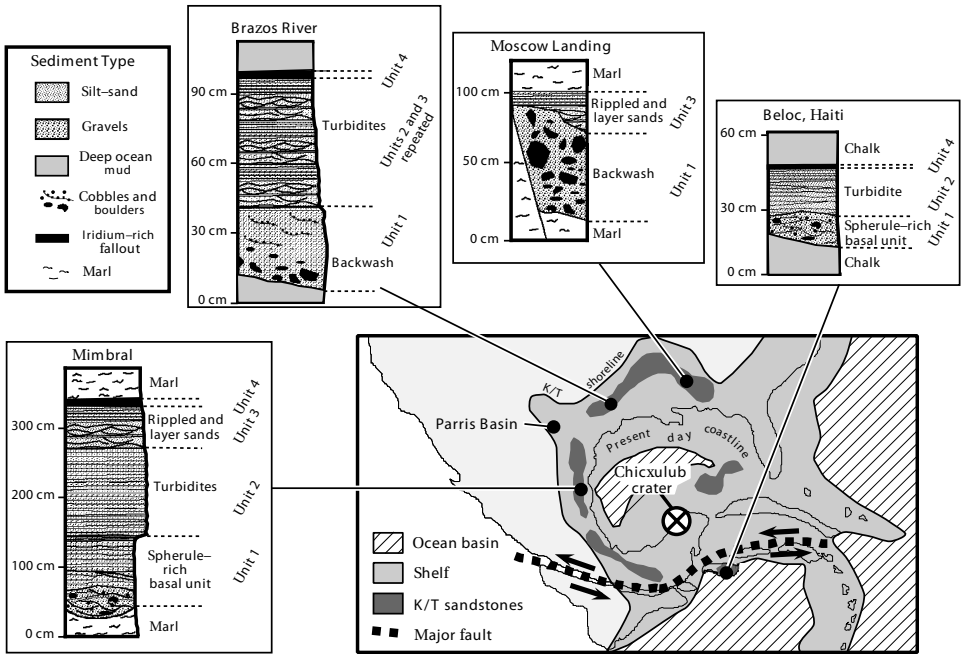

Figure 8.8. Location of the Chicxulub impact crater and stratigraphic sections of tsunami deposits surrounding the proto-Gulf of Mexico. Based on Bourgeois *et al.* (1988), Bohor (1996), and Smit *et al.* (1996).

steeper slopes. Following the impact, sunlight was blocked by an estimated 100×10^9 tonnes of dust thrown into the atmosphere—a process that eliminated photosynthesis for a two- to six-month period. Large amounts of CO_2 and SO_2 were released into the atmosphere together with the formation of equivalent amounts of nitrogen oxides. Subsequent scavenging of these molecules from the atmosphere produced an acid rain rich in sulfuric and nitric acids. All animals dependent upon photosynthesizing organisms became extinct. In total, 38.5% of all genera and 67% of all species disappeared. Only the end of the Permian 250 million years ago saw the extermination of more species.

The evidence for extinction is one of the main signatures of the K/T event left in the geological record. However, the distribution of tsunami deposits up to 9 m thick on continental shelves and the seafloor provide the conclusive proof of an impact event of enormous magnitude. Equations (8.1) and (8.2) indicate that, had the Chicxulub comet fallen into the deep ocean, the tsunami wave would have been over 400 m high 1,000 km from the center of impact. However, the impact occurred on the continental shelf, close to the southern shore of the proto–Gulf of Mexico, which formed an enclosed, shallow sea, 1,500 km in diameter (Figure 8.8). The ejecta curtain, the initial blast wave of compressed air from the impact, and finally an atmospheric blast driven by the release of CO_2 from limestone bedrock, produced

a tsunami 100 m high that rolled into the southern United States (Figure 8.1). Within an hour of the impact, the burning forests that had been flattened and then ignited by the initial blast were picked up, mixed with uncompacted sediment and ripped-up bedrock, and then driven inland hundreds of kilometers over the flat coastal plains adjacent to the proto-Gulf. Backwash re-entered the Gulf as a wave tens of meters high, accompanied by channelized backflow that eroded channels across the wide shelf. This slurry spread along the seabed as a turbidity current, depositing a chaotic mixture of ejecta, bedrock clasts, sand, and terrestrial vegetation across the abyssal plain. Reflection of this wave back and forth across the Gulf ensured that landmasses were repetitively swept by tsunami diminutively over the next few days. Slowly, sediment suspended in the water column and dust put into the atmosphere settled to the seabed over the next few weeks as quiescence returned to a lifeless ocean. This latter sediment contained the iridium-rich signature of the cosmogenic source. Millions of years later as the modern Gulf formed, deposits laid down by the passage of the tsunami were uplifted and then exposed around the Chicxulub impact center—along the Mexican Gulf coast, in exposures on the Brazos River in Texas, at several sites in Alabama, and on the Island of Haiti (Figure 8.8).

The nature of the turbidite signature varies depending upon its proximity to the initial impact and its relative location to the shoreline of the proto-Gulf (Figure 8.8). The deposits have been attributed to turbidity currents generated by submarine slides or to bottom currents generated by the passage of tsunami waves. The enormous height of the wave would have ensured that even the deepest part of the Gulf was in shallow water and that cobble-sized material was moved. However, the passage of the wave over the seabed was only capable of deforming bottom sediment or rearranging the sediment that was already there. In quiescent deep water, this sediment was most likely mud. However, no homogenites similar to those deposited following the eruption of Santorini have been found. All deposits contain sand that must have been brought there from the shelf by backwash generated by the tsunami or by turbidity currents. Because tsunami have wavelengths tens if not hundreds of kilometers long, current velocities at the seabed generated by the oscillatory nature of the wave must have been unidirectional, pointing away from the impact site for several minutes under the crest. This would have been followed by a longer period of reverse flow that decreased in magnitude until the next wave in the tsunami wave train approached. Thus, sandy sediment once deposited in the deep ocean could have been reworked by other waves in the tsunami wave train and by the seiches that followed. In addition, ejecta in the form of spherules are absent or sparse at the base of some deposits. Ejecta present at the base of deposits in the ocean did not necessarily fall there *in situ* from the atmosphere. Because ejecta were thrown high into the atmosphere, it took time for it to settle back to the Earth's surface. During this time the Earth rotated eastward. Thus, most ejecta tended to fall on the shelf to the west of the impact site, forming a layer 1 m thick. Strong tsunami backwash swept these spherules seaward and deposited them first below the subsequent turbidites. Shelf sands then covered the turbidites, leading to a reversal in stratigraphy.

Both the hydrodynamics of the tsunami and the relative abundance of ejecta are reflected in the deposits. At Beloc, on the Island of Haiti, which was in water about

2 km deep at the time of the impact, deposits are thinnest because they are farthest from sources of sand on the shelf. A turbidity current first deposited a layer of ejecta 15 cm–70 cm thick. This grades upward into a deposit of fine sand and silt that is 20 cm thick with low-angled cross-bedding (Figure 8.8). Thin iridium-rich layers of sandy silt 1 mm–2 mm thick occur at the top of the sequence. This upper segment in many locations is disturbed, implying that a second tsunami may have affected the area afterwards. This could have been generated by volcanism triggered by the impact or by subsequent landslides on an unstable seabed. In slightly shallower water, but still offshore of any shelf, west of the impact site at Mimbral where still-water conditions existed on the seabed, fine limestone-rich clays called marls were overlain by 1 m of ripped-up limestone, mixed together with the ejecta debris from the impact zone. These sediments are best preserved in the channels cut by tsunami backwash and are overlain by at least 2 m of sand derived from the distant shoreline and brought to the seabed by turbidity currents. This unit can be traced over a distance of 2,000 km, from Alabama through Texas to the southern border of Mexico. This unit is overlain by a meter of crosscurrent beds of sequential rippled sand and fine clay. In many respects, the deposit has all of the characteristics of a Bouma sequence as described in Chapter 3. Finally, a thin layer, several centimeters thick, caps the sequence. This uppermost layer contains the iridium-rich dust fallout that settled out of the atmosphere over several weeks following the impact. Closer to shore, about 100 km landward of the shelf edge at a site like the Brazos River in Texas, the tsunami wave swept over the muddy, flat shelf, scouring out swales with a relief of 0.7 m. Backwash dominates these sites. The bottom part of the sand deposits is about 1.3 m thick and consists of rounded calcareous cobbles, shell, fish teeth, terrestrial wood debris, and angular pieces of mudstone. At Moscow Landing, Alabama, the shelf was only 30 m deep at the time of impact. Seismic waves preceded the tsunami creating normal faults in a north–south direction. These are paralleled by grooves, flute casts, scour features, and lineations created by the passage of the wave over undular topography molded into soft bottom muds. Here, backwash in the form of undertow wedged the bottom sediments against fault blocks. Boulders are also present in the deposit. The bottom unit fines upward into parallel-laminated and symmetrically rippled sandstone, siltstone, and mudstone. In places, the sequence is repeated up to three times, indicating the passage of more than one wave. The upward part of the sequence, which is iridium-rich, shows evidence of seiching.

The size of mud clasts at the Brazos River site gives some indication of the bottom shear velocities that must have been generated over the shelf. These values are as high as 1 m s^{-1}, far exceeding those that could be generated by storms on a shelf in 50 m–100 m depth of water. The velocities allude to a tsunami wave between 50 m and 100 m high with a period of 30–60 minutes. Boulder deposits indicative of a mega-tsunami are rare; however, they have been found close to the shoreline of the proto-Gulf at Parras Basin in northeastern Mexico and in the mid-south of the United States. At the latter location, anomalous sandstone boulders up to 15 m in diameter have been found 80 m above floodplains on hills that would have been coastal headlands at the time.

Other events

(Gersonde *et al.*, 1997; Mader, 1998)

Chicxulub tends to dominate the public's perception of what a large asteroid or comet impact can do. While this is the biggest event in the last 225 million years, it is not the only one to have generated an impressive tsunami. For example, an event known as the Eltanin Asteroid Event occurred during the Pliocene 2.15 million years ago. This asteroid, estimated to have been 4 km in diameter, plunged into the Pacific Ocean 700 km off the southwest corner of South America and exploded, sending ejecta into the atmosphere. If the object had a density of $3.6\,g\,cm^{-3}$ and struck at a speed of $20\,km\,s^{-1}$, it potentially generated a mega-tsunami—according to Equation (8.6)—at least 30 m in height along nearby coasts in South America and Antarctica. Spreading waves from the impact site would have extended into the North Pacific and Southern Ocean with a deep-water wave height of 10 m reaching the most distant coasts. Conservatively, the resulting tsunami would have been 4 m, 10 m, and 20 m high off the coasts of Japan, California, and New Zealand, respectively. Run-ups would have been amplified by a factor of 2 to 3 times as the wave traveled across continental shelves.

Evidence for this tsunami consists of unusual skeletal deposits of marine and land mammals found mixed on the Peruvian coast, corresponding to the time of the Eltanin impact. In coastal Antarctica, late Pliocene deposits of marine sediments containing continental shelf diatoms have been found several tens of meters above sea level, also dating from this period. The sediment layers are less than 0.5 m thick and are analogous to the splays of shelf sediment described in Chapter 3, onlapped onto coasts by modern tsunami. Finally, the splash from the impact may have lobbed marine diatoms and other microfossils thousands of kilometers into the ice-free Transantarctic Mountains of Antarctica. If this is so, then this evidence may resolve one of the discrepancies between theory and field evidence for the size of cosmogenically generated mega-tsunami—namely, that splash may be a potent force generating some of the geomorphic evidence attributed to catastrophic flows.

DELUGE COMET IMPACT EVENT 8,200 ± 200 YEARS AGO

(Clube and Napier, 1982; Asher and Clube, 1993; Asher *et al.*, 1994; Kristan-Tollmann and Tollmann, 1992)

If cosmogenically generated tsunami are so rare—certainly within the timespan of human civilization—then a paradox exists because evidence for such events certainly appears often in the geological record and in human legends. Traditionally, the difficulty in discriminating between fact and fiction, between echoes of the real past and dreams, has discouraged historians and scientists from making inferences about catastrophic events from myths or deciphered records. Yet, common threads appear in many ancient tales. Stories told by the Washo Indians of California and by the Aborigines of South Australia portray falling stars, fire from the sky, and cataclysmic floods unlike any modern event. Similar portrayals appear in the *Gilgamesh* myth from the Middle East, in Peruvian legends, and in the Revelations of Saint John and

the Noachian flood story in the Bible. Victor Clube of Oxford University and William Napier of the Royal Observatory of Edinburgh have pieced together consistent patterns in ancient writings, which they interpret as representing meteoritic showers 3,000–6,000 years ago. One of the more disturbing accounts has been compiled from these legends by Edith and Alexander Tollmann of the University of Vienna, who believe that a comet circling the Sun fragmented into seven large bodies that crashed into the world's oceans $8{,}200 \pm 200$ years ago. This age is based on radiocarbon dates from Vietnam, Australia, and Europe. The impacts generated an atmospheric fireball that globally affected society. This was followed by a nuclear winter characterized by global cooling. More significantly, enormous tsunami swept across coastal plains and, if the legends are to be believed, overwashed the center of continents. The latter phenomenon, if true, most likely was associated with the splash from the impacts rather than with conventional tsunami run-up. Massive floods then occurred across continents. The event may well have an element of truth. Figure 8.9 plots the location of the seven impact sites derived from geological evidence and legends. Two of these sites, in the Tasman and North Seas, have been identified as having mega-tsunami events around this time. The North Sea impact center corresponds with the location of the Storegga slides described in Chapter 6. Here, the main tsunami took place $7{,}950 \pm 190$ years ago. One of the better dates comes from wood lying above tektites in a sand dune along the south coast of Victoria, Australia. The tektites are associated with the Tasman Sea impact and date at $8{,}200 \pm 250$ years before present. These dates place the *Deluge Comet* impact event—a term used by the Tollmanns—around 6200 BC. This event does not stand alone during the Holocene. It has been repeated in recent times—a fact supported by Maori and Aborigine legends from New Zealand and Australia.

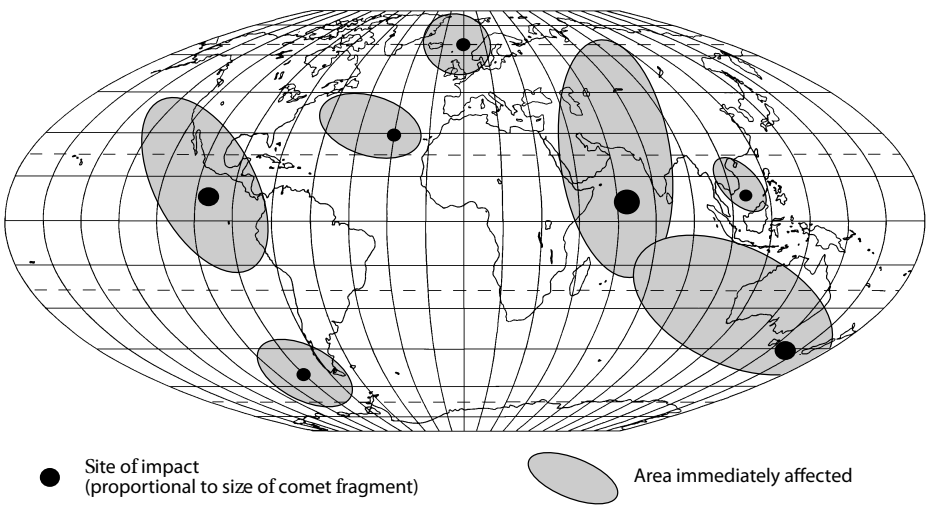

Figure 8.9. Reconstruction of the impact sites of fragments of the *Deluge Comet* $8{,}200 \pm 200$ years ago based on geological evidence and legends. From Kristan-Tollmann and Tollmann (1992).

THE MAHUIKA COMET IMPACT EVENT AND EASTERN AUSTRALIA

(Monzier, Robin, and Eissen, 1994; Steel, 1995; Young *et al*., 1997; Bryant and Nott, 2001; Abbott *et al*., 2003; Matzen, Abbott, and Pekar, 2003; Marcus, Melosh, and Collins, 2005)

The evidence from Australia for cosmogenic mega-tsunami is based upon the magnitude of geomorphic features and their contemporaneous occurrence over a wide region of the Tasman Sea (Figure 8.10B). This chronology coincides with the timing of legends and the influx of comets and asteroids over the last millennium. As pointed out in Chapter 1, Australia historically has not been affected significantly by large tsunami. The closest sources for earthquake-generated tsunami lie along the Tonga–New Hebrides Trenches and the Indonesian Archipelago. An earthquake with a surface wave magnitude greater than 8.3 can be generated in the southwest Pacific every 125 years. The highest tsunami recorded at Sydney since 1870 occurred on May 10, 1877 and had a height of 1.07 m. The Chilean earthquake of 1868 produced a tsunami height of 1.0 m, while the Chilean earthquake of May 22, 1960 generated a tsunami height of 0.85 m. On the west coast, the biggest tsunami

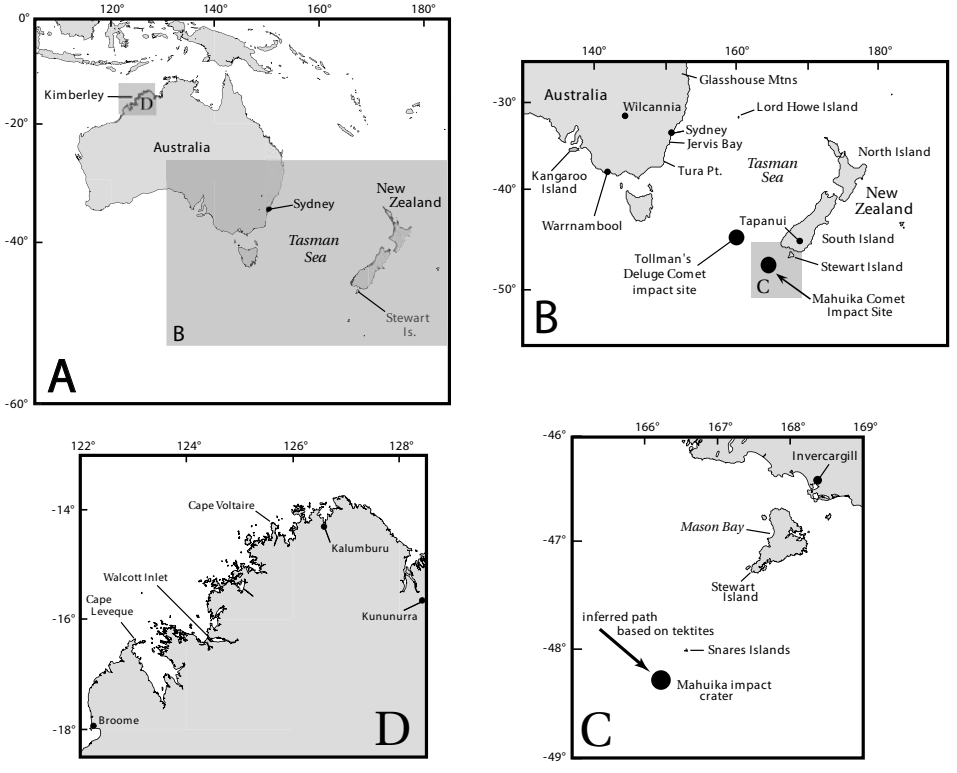

Figure 8.10. Location map of Australia and New Zealand where physical and legendary evidence exists for tsunami.

run-up has been 6 m at Cape Leveque, Western Australia, on August 19, 1977 following an Indonesian earthquake.

Paleo-tsunami, generated by conventional mechanisms and larger than these historical events, are possible. The proximity of the northwest coastline to the volcanically and seismically active Indonesian Archipelago makes large tsunami with run-ups of 10 m a distinct possibility. Additionally, the east coast lies exposed to tsunami generated by earthquakes on seamounts in the Tasman Sea and along the Alpine Fault running down the west coast of the South Island of New Zealand. This latter fault last ruptured in the 15th century before European colonization of the region. Nor can volcanic activity be ruled out along the east coast. Active volcanoes lie in the Tonga–Kermadec Trench region north of New Zealand. In 1452, the eruption of Kuwae volcano in Vanuatu created a crater 18 km long, 6.5 km wide, and 0.8 km deep. The eruption, which was three to four times bigger than Krakatau, produced a tsunami wave 30 m high. Finally, local slides off the Australian continental shelf also cannot be ignored. A very large submarine landslide, mentioned in previous chapters, lies 50 km offshore from the coast south of Sydney. This slide is a prime candidate for the tsunami-deposited barrier described in Chapter 4 along the adjacent coast (Figure 4.2).

The location of a possible comet impact has recently been discovered lying in 300 m depth of water on the continental shelf 250 km south of New Zealand at 48.3°S, 166.4°E (Figure 8.10C). The crater is 20 km in diameter and could have been produced by a comet 1.6 km in size traveling at a speed of 51 km s^{-1} (all calculations based on Marcus, Melosh, and Collins, 2005). When it struck, it would have generated an earthquake with a surface wave magnitude of 8.3. The lack of sediment that normally settles over time from the ocean suggests that the crater is less than 1,000 years old. The comet has been named Mahuika after the Maori God of fire. Tektites found in sediments to the southeast indicate a trajectory for this comet from the northwest, across the east coast of Australia. If the recent age of the event were correct, Aborigines in Australia and Maori in New Zealand would have observed this comet's dying moments.

Geological evidence for mega-tsunami

(Oliver, 1988; Bryant and Young, 1996; Bryant, Young, and Price, 1996; Jones and Mader, 1996; Bryant *et al.*, 1997; Bryant and Nott, 2001; Bryant, Walsh, and Abbott, 2006)

The tsunami produced by Mahuika would have been significant although it is difficult to model the height of the wave accurately because the comet had a density approaching 1.0 g cm^{-3} and struck in shallow water on the continental shelf. The equations used to calculate values in Table 8.1, as a first approximation, yield a tsunami 75 m high at the southern tip of Stewart Island and 5 m high along the coast south of Sydney, Australia. These values may be realistic. From Chapters 3 and 4, four signatures stand out as unique features of cosmogenic tsunami: chevrons (Figure 3.10), imbricated boulders fronting or overriding cliffs (Figure 3.15), whirlpools bored into bedrock (Figure 3.26), and bedrock fluting producing keel-like or

Figure 8.11. Giant flutes cut into granite on the southern headland of Mason Bay, Stewart Island, New Zealand. The flutes point back to the Mahuika comet impact site. The flutes are over 40 m high and were cut by vortices in flow as the tsunami went over the headland. Photo credit: Dr. Dallas Abbott, Lamont-Doherty Earth Observatory, Columbia University.

cockscomb-like features (Figures 3.24 and 4.14). Along the south and west coast of Stewart Island whirlpools and giant flutes have been eroded into granite. The flutes at the southern end of Mason Bay where the tsunami wave theoretically had a height of 60 m rise to a height of 20 m and clearly indicate that the headland was overtopped (Figure 8.11). The orientation of the flutes point directly to the Mahuika impact site. Some of the geological evidence for cosmogenic tsunami along the east coast of New South Wales, Australia has already been presented. Of additional interest are other boulder deposits found in the region, namely at Gum Getters Inlet and Mermaids Inlet. At Gum Getters Inlet, angular boulders 6 m–7 m in diameter have been stacked up to 30 m above sea level into a small indent cut into the cliffs (Figure 8.12). It would be tempting to attribute this debris to cliff collapse but for the fact that the imbricated blocks rise to the top of the cliffs and there is no evacuation zone upslope. The deposit is all the more unusual in that the site is virtually protected from dominant southeast storm swell. Imbricated blocks of similar size choke the entrances of two narrow and deep gulches at Mermaids Inlet (Figure 8.13). Some of the largest blocks, which are over 5 m in length, have not simply dropped from the cliff faces but have been rotated 180° and shifted laterally in suspension flow. The depth of overland tsunami flow in the Jervis Bay region has been theorized at 9.5 m. The boulder features at Gum Getters Inlet are suggestive of even greater flow depths of 15 m–20 m, which only

Figure 8.12. Imbricated boulders stacked against a 30 m high cliff face on the south side of Gum Getters Inlet, New South Wales, Australia. Some of these boulders are the size of a boxcar. Note the person circled for scale.

a cosmogenic tsunami could generate. Just as dramatic are the dunes at Crocodile Head, Jervis Bay described previously in Chapter 3. They lie atop 80 m high cliffs, have a relief of 6.0 m–7.5 m, are spaced 160 m apart, and are akin to the undulatory to linguoidal giant ripples that are features of catastrophic flow similar to that observed in the scablands of Washington State. The flow over the dunes at Crocodile Head is theorized to have been 7.5 m–12.0 m deep and to have obtained velocities of $6.9\,m\,s^{-1}$–$8.1\,m\,s^{-1}$. The direction of the tsunami producing this mega-ripple field came from the south Tasman Sea.

Finally, there is evidence on this coast of tsunami run-up higher and farther inland than produced by conventional processes. Historically, the largest run-up produced by a volcano was 90 m on August 29, 1741 on the west coasts of Oshima and Hokkaido Islands, Japan. Santorini may also have had a tsunami wave height of 90 m, but confirmed evidence for its run-up does not exceed 50 m above sea level. The

Figure 8.13. Boulder pile blocking the mouth of Mermaids Inlet, New South Wales, Australia. The largest blocks are more than 5 m in length. The gulch on the right contains a shelly beach dated at 1790 ± 70 radiocarbon years BP.

largest tsunami run-up generated by an earthquake was 100 m on Ambon Island, Indonesia, on February 17, 1674. In recent times, an earthquake or submarine landslide off the Sanriku coast of Japan produced a run-up of 38.2 m on June 15, 1896. The tsunami that struck Flores Island on December 12, 1992 had a run-up of 26.2 m at Riang–Kroko (Figure 3.6). In contrast, the highest paleo-tsunami run-up identified along the south coast on New South Wales so far is 130 m at Steamers Beach, Jervis Bay, on the crest of a chevron dune. This site has been referred to often in this text. However, this limit is underestimated because the wave still had enough force not only to flow over the headland and into Jervis Bay, but also to transport large boulders along a ramp inside the bay. Conventional processes generating tsunami cannot explain the geomorphic features evident along the southeast coast of Australia.

Maori legends supporting a cosmogenic event

(Tregear, 1891; Steel and Snow, 1992)

One of the more intriguing legends supporting a cosmogenic impact in the southwest Pacific is the New Zealand Maori legend known as the *Mystic Fires of Tamaatea (Tamatea)*. *Tamatea* is a very ancient person. He was the fifth in descent from Rangi, the Sky. The legend originates in an older legend related to some volcanic catastrophe or conflagration before the Maori came to New Zealand. It was transferred via the North Island to the Southland and Otago regions of the South Island, centered on the town of Tapanui (Figure 8.10b). Here there appears to be evidence for an airburst that flattened trees similar to the Tunguska event. The remains of fallen trees are aligned radially away from the point of explosion out to a distance of 40 km–80 km. Local Maori legends in the area tell about the falling of the skies, raging winds, and

mysterious and massive firestorms from space. The Sun was screened out, causing death and decay. Maori names in the region refer to a Tunguska-like explosion. Tapanui, itself, translates locally as "the big explosion". In *The Maori–Polynesian Comparative Dictionary* compiled by Tregear (1891) and based on over 160 references that trace Maori terms back to their Polynesian sources, Tapanui means "to split" or "to pulverize soil". Waipahi locally means "the place of the exploding fire". Place names such as Waitepe*ka*, *Kaka* Point, and Owe*ka* contain the southern Maori word *ka*, which in *The Maori–Polynesian Comparative Dictionary* means "to burn, to be lighted, to take fire", while *kaka* means "red-hot". Some place names put the timing of the fires in the Southern Hemisphere winter around June at the timing of the Taurids. A deluge then followed the widespread fires. One legend states that the Aparima Plains west of Invercargill were flooded. Maori place names such as *Tai*nui, *Tai*roa, and Pare*tai*, inland from the ocean, suggest that a tsunami was involved because the affix *tai* can be translated as *wave*. The Maori also attribute the demise of the moas, as well as their culture, to an extraterrestrial event. The extinction of the moa is remembered as Manu Whakatau, "the bird felled by strange fire". One Maori song refers to the destruction of the moa when the horns of the Moon fell down from above. On the North Island, the disappearance of the moa is linked to the coming of the man/god *Tamaatea* who set fire to the land by dropping embers from the sky. Remains of moa on the South Island can be found clustered in swamps as if these flightless birds fled *en masse* to avoid some catastrophe. Southern Maori legends tell of stones falling from the sky that caused massive firestorms that not only annihilated the moa, but also Maori culture.

Aboriginal legends supporting a cosmogenic event

(Peck, 1938; Jones and Donaldson, 1989; Flood, 1995; Johnson, 1998; Cahir, 2002; Bryant, Walsh, and Abbott, 2006)

This book began with a story based upon Aboriginal legends about a comet/asteroid impact. Many of these legends are concentrated in the southeast corner of Australia, where some of the best signatures of large tsunami are preserved. As with Gervasse's description of the meteor impact with the Moon on June 19, 1178, the Aboriginal legend in Chapter 1 mentions that the Moon rocked. There are also similarities with the Maori legend of the *Fires of Tamaatea*. In both, stars, fire, and stones fell from the sky, and there was a thunderous explosion. Farther inland in New South Wales, the Paakantji tribe, near Wilcannia on the Darling River (Figure 8.10b), also tell of the sky falling. A great thunderous ball of fire descended from the sky, scattering molten rock of many colors. As in the Maori legend of New Zealand, floods then followed this event. The floods may have been the consequence of millions of tonnes of seawater, vaporized by an asteroid impact with the ocean, condensing and falling as rain. Other tsunami and comet legends that could relate to the Mahuika comet occur along the eastern coast of Australia. On the north coast of New South Wales, Aborigines speak of "the Moon setting in the east" and of flooding of rivers such as the Namoi from the ocean on a clear day. A spear from the sky fell into the sea followed by a great flood that changed the coastline. Individual large boulders on

rock platforms are also identified as representing particular Aborigines struck down by a large wave. In southeast Queensland, the Glasshouse Mountains, which lie at the western side of the coastal plain 20 km from the ocean, represent ancestral forms of Tibrogargan and his family. Tibrogargan one day was alarmed to see a great rising of the ocean and fled inland with this family. Individual peaks in the Glasshouse Mountains represent his family still gazing seaward at the threat.

In South Australia, another legend tells of stars falling to Earth to make the circular lagoons fringing the coast. In addition, the legend of Ngurunderi clearly alludes to tsunami. Ngurunderi was a great ancestral figure of the southern tribes in South Australia, who established tribal laws. His two wives ran away from him and he angrily went after them, eventually catching up with them at Cape Jervis just as they were about to wade from Kangaroo Island to the mainland (Figure 8.10b). To punish his wives he ordered the waters to rise up as a tidal wave and drown them. The waters came in with a terrific rush and roar, carrying the women toward the mainland. They tried frantically to swim against the tidal wave but drowned. Their bodies were turned to stone and are seen as two rocks off the coast of Cape Jervis, called the *Pages* or the *Two Sisters*. The history of Aboriginal occupation of Kangaroo Island remains enigmatic. The island shows extensive evidence of Aboriginal occupancy; but, when the first European—Matthew Flinders—landed on the island in 1802, it was unoccupied. Mainland Aborigines call Kangaroo Island, Kanga—the Island of the Dead. The coastline also evinces signatures of cosmogenic tsunami. Most significant are enormous whirlpools on the northern coast of the island, where the Aboriginal legend is set. The features are larger than those found at Atcheson Rock (shown in Figure 3.26).

Perhaps the most intriguing legend along the southeast coast of Australia is the story of the eastern sky falling. Aborigines south of Sydney believed that the sky was held up on supports and that these gave way on the eastern side. One version refers to the ocean as belonging to the sky. The ocean had fallen down, wiping out Aboriginal culture. Some tribes were even requested by others to send tribute to the east to be given to the spirit people in charge of holding up the sky so that it could be repaired. Archeological evidence for tsunami and their impact on Aboriginal culture also exists along this coast. One of the depositional signatures of tsunami mentioned in Chapter 3 was the presence of disturbed Aboriginal kitchen middens, which form a special case of dump deposit more than 10 m above sea level on some rocky headlands. At Atcheson Rock, 60 km south of Sydney (Figure 3.23), tsunami overwashed a 20 m to 25 m high headland, boring whirlpools into the sides. The wave was traveling so fast that it separated from the headland and made contact with the sea 100 m–200 m on the lee side in a bay. Flow separation caused profuse amounts of coarse sediment to drop from the flow under gravity. This was sediment deposited on the lee side of the headland. On the far side of the bay, a dump deposit contains numerous silcrete hand axes and shaped blades that came from an Aboriginal camp at the head of the embayment. Aborigines in this camp initially would have heard, but not seen, the tsunami approaching. Their first indication of disaster would have been when they looked up and saw the ocean dropping down on them from the sky as the tsunami wave surged over the headland.

Timing of Mahuika

(Mooley *et al*., 1963; Bowdler, 1976; Hasegawa, 1979, 1992; Sullivan, 1987; Sekanina and Yeomans, 1984; Talandier and Bourrouilh-Le Jan, 1988; Attenbrow, 1992; Steel and Snow, 1992; Young and Bryant, 1992; Weisler, 1996; Stuiver *et al*., 1998; McGlone and Wilmshurst, 1999; Bryant and Nott, 2001; Burney *et al*., 2001; Nichol, Lian, and Carter, 2003; Baillie, 2006)

It is possible to constrain the age of a regional cosmogenic mega-tsunami event and with it many associated Aboriginal and Maori legends using six separate lines of evidence. First, it is possible to surmise the most likely time of asteroid and comet impacts over the last two thousand years using a combination of Chinese, Japanese, and European records of meteor, comet, and fireball sightings. Figure 8.3 plots the accumulated record, up to the beginning of the 19th century when scientific observations began in earnest. A quasi-cyclic pattern is evident in the comet-sighting records that can be linked to the dominance of the Taurid complex in the inner solar system. As discussed at the beginning of this chapter, this complex formed from the breakdown of a giant comet that entered the inner solar system about 15,000 years ago. By far the most active period of the past two thousand years happened between 1401 and 1480.

Second, 29 radiocarbon dates have been obtained from marine shell found along the New South Wales coast in disturbed Aboriginal middens, deposited in tsunami dump deposits and sand layers, and protected beneath boulders transported by tsunami. Of these, three samples were obtained from Lord Howe Island situated in the Tasman Sea halfway between Australia and New Zealand (Figure 8.10). Radiocarbon dates do not simply represent a calendar age. Each can be plotted as a frequency distribution over a span of radiocarbon years. An example of this is shown in Figure 8.14a for four radiocarbon dates of shell taken from a deposit. The distributions have then been summed in Figure 8.14b to show the most likely age of the deposit centered on the highest peaks in the combined distribution. In this example, the deposit does not have one defined age but several "probable" ones centered at 1100, 1400, and 1600. This variation is typical of marine deposits because they can incorporate old, as well as recent, shell. Radiocarbon dates do not match calendar ones. They have to be converted. This can be done using a carefully constructed calibration table based on marine species (Stuiver *et al*., 1998). Conversion of the data in Figure 8.14b is shown in Figure 8.14c. The latter shows five problems with radiocarbon dating. First, most marine shells absorb old radiocarbon stored in the oceans. Marine shells tend to be 400–500 years too old! Hence when their age is converted to a calendar age, it is shifted forward in time. Second, this shift means that radiocarbon dating cannot be carried out for any shell that has grown since 1770. The age comes out as modern. Third, radiocarbon production in the atmosphere varies over time. This can lead to age reversals. Unfortunately, age reversals plague the last two millennia. Thus, radiocarbon dates cannot be converted to calendar ones simply by subtracting 400–500 years. This is evident in Figure 8.14c, where the peaks in the summed radiocarbon distributions have not shifted by the latter amount into the future, but now appear at 1300, 1450, and 1700. Four, nor can

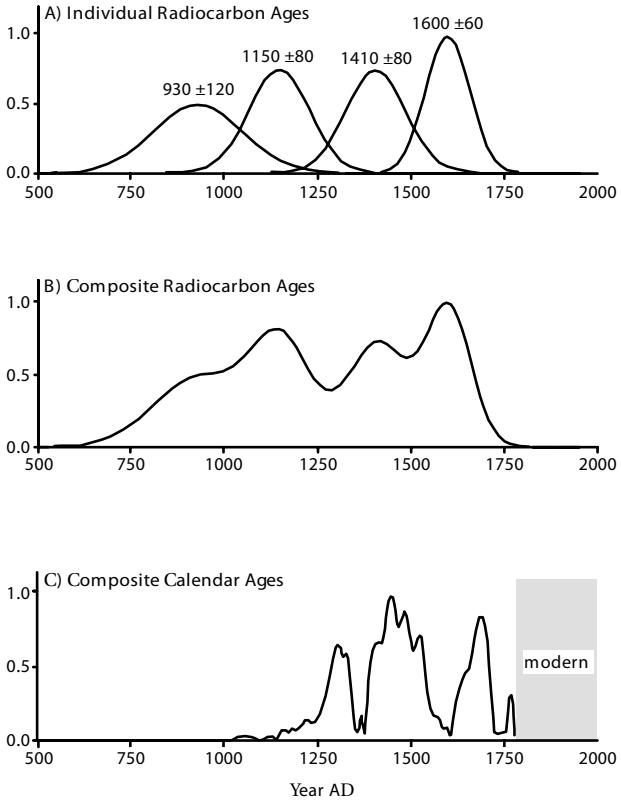

Figure 8.14. Schematic representation showing the steps in converting radiocarbon ages to calendar ones and plotting the results as an age distribution over time. Data on the *y*-axis scaled to a maximum value of one.

any peaks in the resulting distribution be interpreted as the likely time for an event because age reversals leave gaps that artificially create peaks in a calendar-age distribution. For example, no matter how many marine shells one dates, one will never get a calendar age of 1380. An age reversal in radiocarbon around this time produces a gap and prevents the age of any shell growing at this time from being determined. Finally, the conversion of radiocarbon age distributions to calendar ones introduces a lot of noise. This can make the identification of prominent peaks difficult.

Our 29 dates are all less than 2,000 years old. Their summed calendar-age distributions are presented in the bottom panel of Figure 8.3. For presentation purposes, the highest value has been standardized to a maximum of one. The most prominent peak centers on 1500 ± 85. However, this peak is most likely an artifact. All that can be stated from the time series is that there is a 95% probability that a cosmogenically induced mega-tsunami event occurred in the Tasman Sea between 1200 and 1730. This corresponds with the largest number of asteroid

observations for the past two millennia and a peak in observable comets. As well, a date on marine shells in the tsunami deposit at Atcheson Rock that accounts for the Aboriginal legend of the ocean falling from the sky occurs within this timespan. The timing for a major impact during this period is also supported by a radiocarbon date from Stewart Island, New Zealand—the closest large landmass to the Mahuika impact site. The date was obtained from pipi shell (*Paphies australis*) located about 500 m inland and 30 m above sea level at Mason Bay on the west coast of Stewart Island. It yielded a calibrated age of 1301 ± 36.

The third line of evidence is circumstantial. A major environmental event that disturbed coastal Aboriginal culture in eastern Australia occurred between 1200 and 1730. For example, a disturbed midden has been found 30 m above sea level within Sydney Harbor. This is beyond the run-up of modern storm waves in the harbor. The date of this deposit is 1448. There is also clear evidence that Aborigines switched from collecting large mollusks to fishing about 500–700 years ago. Instead of continuing their profuse gathering of marine shells for food, Aborigines switched to fishing. If a tsunami wave had the force to sweep over 130 m high headlands in the region, then it would have been powerful enough to clear all marine shells from rock platforms. The event necessitated a change in lifestyle by Aborigines simply to survive starvation. Middens at various sites along the south coast of New South Wales also indicate that edible mussels originating from more protected tidal inlets began to replace gastropods originating from rock platforms concomitantly with the switch to shell fishhooks. At Bass Point, which is dominated by mega-tsunami erosion and which is a headland conducive to the legend of the ocean falling from the sky, the change occurred around 1380. There is also evidence from increased usage of rock shelters that Aborigines moved inland around this time. While interpreted as an indication of increasing population, it could also indicate abandonment of a dangerous coast.

Fourth, it is possible to pin down the approximate age of the *Fires of Tamaatea*. The cosmic fires reported in Steel and Snow (1992) burnt vegetation across the South Island. There are two sources of organic material for radiocarbon dating this event: buried charcoal and carbon derived from peats in swamps and bogs that have been burnt. This material traditionally has been interpreted as reflecting the time of deforestation due to Maori occupation in New Zealand. However, much of the burnt material comes from uninhabitable high country that was burnt on a vast scale. Figure 8.3 also plots the distribution of these dates, which spans at least two centuries and terminates at the end of the 15th century. This wide range in dates is logical knowing that mature trees, already hundreds of years old, burnt. The crucial point is that few ages occur after the 15th century concomitant with the peak in meteorite and comet observations.

Fifth, the Mahuika comet may not have been a single impact, but been widespread throughout the southwestern Pacific Ocean. Pertinent are four radiocarbon dates obtained from the marine shell *Paphies subtriangulatum* from a tsunami dump deposit on the eastern side of Great Barrier Island, New Zealand (Figure 8.10c). The deposit consists of a massive sheet of gravel, cobble, sand, and shell rising to a height of 14.3 m above present sea level and extending up to 300 m inland. A composite calendar-age of AD 1400–AD 1700 with a 95% confidence interval was obtained from

these samples. Also of relevance is the age of a tsunami deposit found in the Mahaulepu Caves on the south coast of Kauai Island, Hawaii, 7,300 km northeast of the New Zealand deposit. The caves lay 7 m–8 m above sea level. They are filled by an 80 cm thick massive deposit of gravels, organic debris, and boulders. Some of the boulders weigh over 100 kg. Four radiocarbon dates obtained from seed and rind material (*Aleurites* and *Lagenaria*, respectively) yielded an age between 1480 and 1610.

Finally, there is substantial evidence that a comet struck the Earth at the end of the 15th century. The small and not very active comet X/1491 B1 (formerly 1491 II) was seen by Korean astronomers in the evening sky of January 20, 1491. This comet appears to have been a Jupiter family object with a period of less than 20 years. The Koreans followed the comet's movement in the constellation Cetus and last sighted it brightly on February 12. It had disappeared by the 14th. According to calculations by Hasegawa (1979), X/1491 B1 was making a close approach to the Earth. Sekanina and Yeomans (1984) calculate that a collision with the Earth was possible on February 13. From the perspective of the east coast of Australia, this comet approached the Earth around midnight from the northwest, most likely at a 45° angle to the horizon. The direction, season, and time of day agree with statements made in Aboriginal legends. The year agrees with the main peak in our radiocarbon dates on shell taken from tsunami deposits along the New South Wales coast. Baillie (2006) also recognized the potential of this comet for an impact with the Earth. He points out that its timing matches the largest ammonium spike in a millennium in Antarctic ice cores that can be interpreted as the signature of a comet impact.

The *Fires of Tamaatea* legend may well have a cosmogenic origin. The timing of the fires is coherent with the dating of mega-tsunami deposits along the adjacent coastline of Australia and New Zealand. Dating evidence indicates that a mega-tsunami associated with a comet impact most likely occurred in this region in the 15th century. The best candidate appears to be comet X/1491 B1, which struck the southwest Pacific late in the evening on the February 13, 1491. The fact that a tsunami can be detected in both Hawaii and New Zealand around the same time may have wider implications for the South Pacific Ocean. The Polynesians colonized the islands of the South Pacific between 1000 and 1500. At least 13 islands were settled and then abandoned unexpectedly during the 16th century including the Marquises, Huahine, Raiatea, and Scilly Islands in French Polynesia. The cause of this abandonment has yet to be explained fully.

EVENTS IN THE KIMBERLEY, WESTERN AUSTRALIA

Legends supporting cosmogenic tsunami

(Crawford 1973; Mowaljarlai and Malnic, 1993; McCafferty and Baillie, 2005)

Legends that can be associated with cosmogenic tsunami also exist in Western Australia, especially in the Kimberley region where, as described in Chapter 4, the biggest mega-tsunami to affect Australia occurred just before European occupation.

Figure 8.15. Comet Rock, Kalumburu, Western Australia. The tail of the rock is orientated 310° to the NW. The painting of the comet is Wandjinan in age. This rock lies about 5 km from the ocean on a plain covered in a layer of beach sand. See color section.

Curiously, when Europeans made contact with Aboriginal coastal tribes in Western Australia, they noted that the Aborigines avoided the coast and made little attempt to use it for food, even though there was evidence of past usage in the form of large shell kitchen middens. The coast appeared to have been abandoned. Legends about tsunami are most notable around Walcott Inlet (Figure 8.10d). Here legends recount a very fast flooding from the ocean that filled this inland tidal body for up to 12 hours. Other myths imply that water flooded to the top of the 500 m high mesas surrounding this inlet. The flooding was extensive from Walcott Inlet in the south, to Kalumburu in the north, and to Kununurra in the east. There is also the intriguing naming of Comet Rock at Kalumburu (Figure 8.15). Here, not only does the rock look like the head of a comet with an extending trail, but there is also an Aboriginal rock drawing on the lower face of the rock that mimics the form of the rock and that is orientated parallel to the rock feature. This rock is orientated 310° to the NW, matching the direction of approach of mega-tsunami on the coast to the west.

Most intriguing are the Wandjina rock art paintings and their associated interpretations. Wandjina paintings are stylistic across the Kimberley. None is older than four centuries. The paintings typically show a clown-like face painted white surrounded by an outer, barbed red halo that represents lightning (Figure 8.16). They are without a mouth and their nose indicates where the power flows down. The Wandjina are the rain spirits of the Wunambul, Wororra, and Ngarinyin

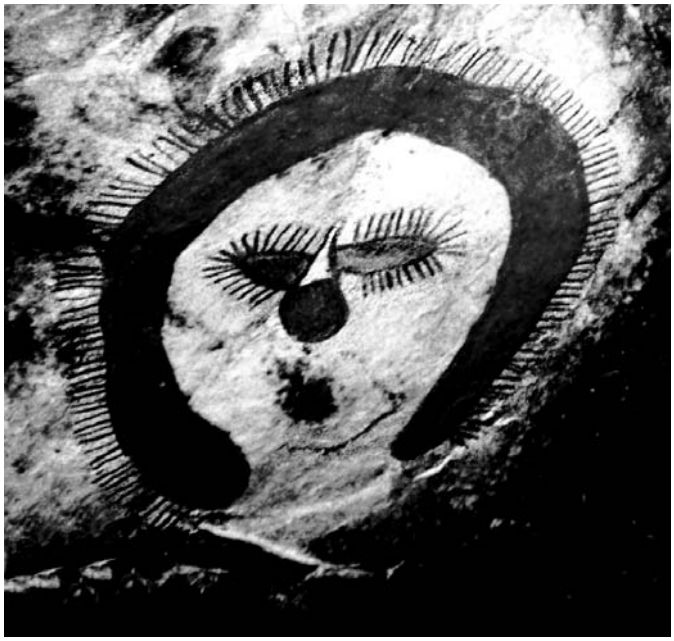

Figure 8.16. A typical Wandjina face painted on rock shelters throughout the Kimberley. The barbed hood represents lightning. Wandjina do not have a nose or mouth. The comet-like symbol in place of the nose represents power. Wandjina do not need a mouth because their knowledge is greater than what can be spoken. See color section.

language people. The Wandjina have great power and are associated mystically with creation and flooding rain. Wandjina do not have a mouth because their knowledge is beyond speaking. Were they to have a mouth, floods would be generated that would drown the whole Earth. Their origin may be much older and traceable to the flood myths in the Dreamtime. Although linked to the annual monsoon, the Wandjina depict something much more intense. Paintings of the Wandjina may be representations of a comet. Far from the modern perception of comets being white and consisting of a nucleus and a single curved tail, comets can take on many shapes and colors. For instance, a comet can form two tails, giving it the appearance of a figure with long flowing hair on two sides. The area around the nucleus can also fragment into many different shapes. Compare the Wandjina rock painting in Figure 8.16 with that of Comet Donati of 1858 in Figure 8.17. The resemblance is striking. Comet Donati developed a human-like head with "eyes" centered on its nucleus or "nose". The nose in the Wandjina painting in Figure 8.16 even looks like a comet. Just like the Wandjina, Comet Donati did not have a "mouth". The Wandjina paintings are not of Comet Donati, but their resemblance to it suggests that they are comet paintings. One Aboriginal legend tells about a flood that was brought on by the "star with trails". The Wandjina caused a great flood that started in the north of Australia and flooded the whole country. Just as quickly as the land was flooded, it

Figure 8.17. Donati's comet of 1858. The image is of the nucleus as the comet approached the Sun. Note the anthropomorphic characteristics of two eyes, a nose, flowing hair, but no mouth. *Source:* McCafferty and Baillie (2005).

drained. The Wandjina spirits came out of the sky or the sea and fought a battle with the Aborigines that the Wandjina won. The fights were repetitive. As well, the Wandjina fought amongst themselves. The Wandjina were also associated with life after the widespread tsunami-like flood event in Walcott Inlet referred to above. Today they control the monsoon with its heavy rain, thunder, lightning, and floods.

Field evidence

(Nott, Price, and Bryant, 1996; Nott, 2004; Bryant, Young, and Price, 2006)

The Kimberley region is subject to some of the most intense tropical storms in the world associated with winds in excess of 300 km h^{-1} and storm surges of 3.6 m. The Kimberley craton is remarkably stable and presently unaffected by large earthquakes. However, its sandstone surface is covered in boulders. These rocks are weathering features resulting from long-term erosion during the Holocene. There is a tendency for isolated boulders to form trains that in some cases contain blocks leaning against each other like fallen dominoes. Something recently not only has shaken the landscape but also cast boulders against each other in an ordered fashion. The orientation of these "castaway" boulders is 350° to the northwest. We propose that the alignment

of shaken boulders reflects the direction of the blast wave from a cosmic airburst. In addition, there is evidence of catastrophic erosion of relatively small streams that is similar to that observed elsewhere across the northern Australian monsoon region. In one of the streams—where the modern channel is less than 70 m wide and 2 m deep—the flood channel is more than 500 m wide with not only evidence of boulders being transported in suspension by flows more than 4 m deep, but also with sufficient intensity to sculpture out erosional features characteristic of the vortices eroded under catastrophic flow described in Chapter 3. These channel widths appear recent and beyond the capacity of maximum probable rainfalls, which are the upper criteria for modern floods. Rainfall induced by a comet impact with the ocean can generate the excessive rainfalls required to carve these channels.

Two sites stand out as showing evidence of tsunami. The first is located at Cape Voltaire directly west of Kalumburu. Here, waves beyond the capacity of cyclones have truncated the ends of headlands. This erosion was not controlled by bedrock lithology or structure as exemplified by the erosion of columnar basalt on the headland. Tsunami erosion on the exposed side of the headland created a ramp that cuts across the dominant structural control that normally would have influenced coastal landforms (Figure 8.18a). This ramp terminates about 20 m above sea level. It would be tempting to attribute the excavation of the ramp to storm waves, but for one additional factor. Little debris evacuated from the ramp is present either on the ramp surface or offshore. Instead, the columnar basalt has been broken into 5 m lengths, tossed over the 40 m high headland and deposited on the sheltered lee slope above the influence of storm waves such that individual blocks reflect the direction of flow, 350° to the northwest (Figure 8.18b). The second site is farther south at Walcott Inlet where the best Aboriginal legend for a tsunami exists. Here, at Collier Bay, a tsunami has infilled an embayment with a mixture of sand, gravel, and shell that rises at least 6 m above the swash or storm surge limit of tropical cyclones. Everywhere in the Kimberley, the coastline has either the erosional effect of a catastrophic wave or its depositional residue in sheltered embayments.

It is possible to date the timing of this mega-tsunami in the Kimberley using radiocarbon dating of shell (Figure 8.19). Again, the same methodology presented in Figure 8.14 was used to calibrate the ages. Fifteen dates exist along the northwest Australian coastline with two from the Kimberley region. The most recurrent age centers between 1620 and 1730 with a defined peak at 1690 indicating that the effects of a mega-tsunami that occurred around the end of the 17th century can now be traced along 1,500 km of coastline. This age agrees with the age of the Wandjina paintings. Based on the evidence presented here, and because Aboriginal legends concentrate on the three main elements of a comet impact in the ocean—the comet itself, tsunami, and flooding rains—this tsunami has been labeled the Wandjina event. No impact crater has yet been found, although attempts are being made to find it. The Wandjina event generated the biggest and most widespread mega-tsunami yet found in the Australian region. The wave reached a maximum of 35 km inland in the Great Sandy Desert, deposited sands up to 40 m deep on the lee side of headlands, and laid down bedded gravels on the landward side of 40 m hills situated over 5 km inland. These aspects are an order of magnitude greater than that produced by any

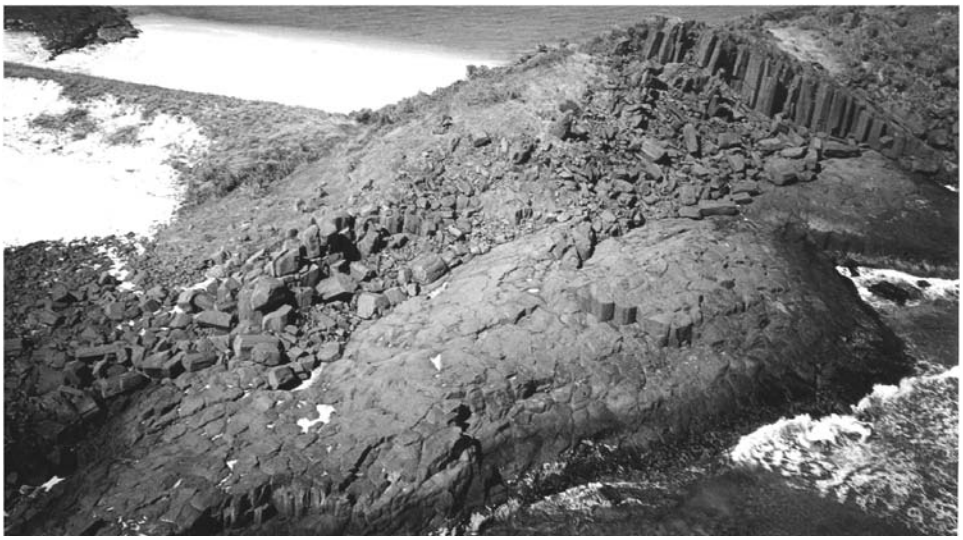

(A)

(B)

Figure 8.18. The basalt headland at Cape Voltaire. (A) The northern side of the headland. Tsunami flow has cut a smooth, undular ramped surface across columnar basalt. Note the scarcity of debris evacuated from this quarry. (B) The debris eroded from the north side of the headland has been transported by the tsunami to the lee of the headland sheltered from cyclone waves. The columnar basalt blocks are aligned with the direction of flow—350º northwest.

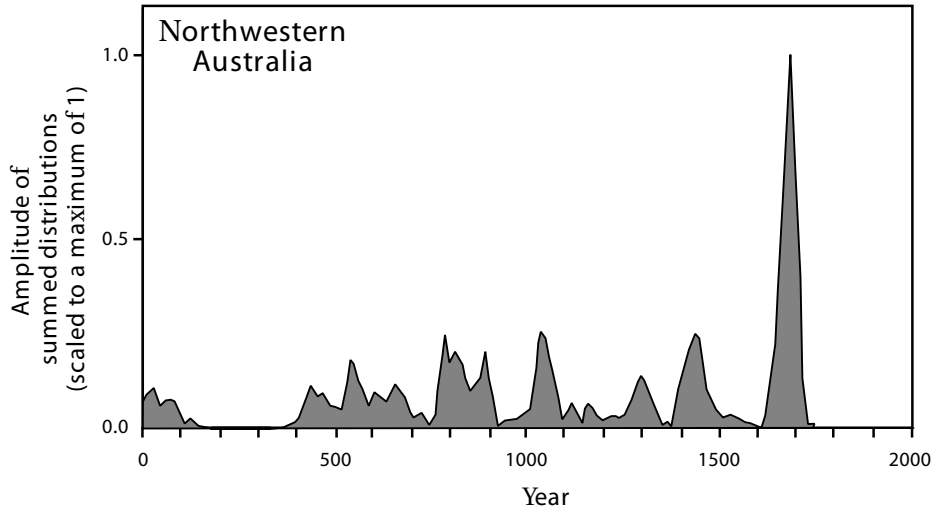

Figure 8.19. The chronology for mega-tsunami in northwestern Australia over the past two millennia. The panel was constructed using the same procedure as used in Figure 8.3. Fifteen dates have been used here. The dips are an artifact of age reversals in radiocarbon chronology.

historic volcanic or earthquake-generated tsunami originating from Indonesia. The 16th and early 17th centuries were a period of European exploration and trade in the region. This event must have been observed and recorded by them. At present no record has been found.